Vivo-Vilches, J., Bailón-García, E., Pérez-Cadenas, A., Carrasco-Marín, F., & Maldonado-Hódar, F. (2013). Tailoring activated carbons for the development of specific adsorbents of gasoline vapors. *Journal of Hazardous Materials*, 263 (Part 2), 533-540.

DOI: 10.1016/j.jhazmat.2013.10.012

Tailoring activated carbons for the development of specific adsorbents of gasoline vapors

J.F. Vivo-Vilches, E. Bailón-García, A.F. Pérez-Cadenas, F. Carrasco-Marín,

F.J. Maldonado-Hódar *

Departamento de Química Inorgánica. Facultad de Ciencias. Universidad de Granada. 18071. Granada. Spain.

*Corresponding Author. Tel: + 34 958240444. Fax: +34 95824852

E-mail address: fjmaldon@ugr.es (F.J. Maldonado-Hódar)

Abstract

The specific adsorption of oxygenated and aliphatic gasoline components onto activated carbons (ACs) was studied under static and dynamic conditions. Ethanol and n-octane were selected as target molecules. A highly porous activated carbon (CA) was prepared by means of two processes: carbonization and chemical activation of olive stone residues. Different types of oxygenated groups, identified and quantified by TPD and XPS, were generated on the CA surface using an oxidation treatment with ammonium peroxydisulfate and then selectively removed by thermal treatments, as confirmed by TPD results. Chemical and porous transformations were carefully analyzed throughout these processes and related to their VOC removal performance. The analysis of the adsorption process under static conditions and the thermal desorption of VOCs enabled us to determine the total adsorption capacity and regeneration possibilities. Breakthrough curves obtained for the adsorption process carried out under dynamic conditions provided information about the mass transfer zone in each adsorption bed. While n-octane adsorption is mainly determined by the porosity of activated carbons, ethanol adsorption is related to their surface chemistry, and in particular is enhanced by the presence of carboxylic acid groups.

Keywords: Activated carbons, surface chemistry, porosity, VOC adsorption, thermal desorption, breakthrough curves.

1. Introduction

The control of volatile organic compound (VOC) emissions is today one of the most difficult environmental challenges. VOC emissions are produced in many different industrial or domestic processes causing serious damage to health, materials and the environment. Both destructive (oxidation) and recovery (adsorption, condensation) techniques are described in the bibliography [1-5] depending on the source of the VOC and its concentration. Emissions associated with the use of fuels in vehicles are of particular importance and there is a clear need to develop effective technologies and strategies to improve the quality of the air we breathe. A lot of research has been done for example on improvements to tailpipes for exhaust gas decontamination [6, 7]. Wang et al. [8] identified a total of 57 individual VOCs in the exhaust gas of gasoline vehicles. Historically, less attention has been paid to evaporative emissions produced during fuel storage and/or transfer. Nevertheless, a number of papers have been published also on this topic [9,10]. For example, Yamada quantified evaporative emissions as the sixth highest source of VOC in Japan, with 4.6 % of total VOC emissions [9]. Specific devices (canisters) for adsorbing VOCs have been developed, which mainly use activated carbons as the adsorbent [11-13]. Furthermore, the American Petroleum Institute (API) has continuously pointed out the effects of these vapors on the environment, health and safety [14], analyzing tank and pipeline regulations to ensure the safe transport, storage and disposal of gasoline.

In recent years there has also been increasing interest in ethanol-based fuels all over the world. The addition of ethanol to gasoline is interesting from an environmental and economic point of view since it can be produced from biomass. Moreover, ethanol is added to gasoline as an anti-knock agent because it is less harmful than MTBE and

ETBE. However, the presence of ethanol in fuels is the subject of controversy, since some studies have proved that ethanol-based fuels produce larger quantities of evaporative emissions [15, 16].

Some empirical models have been developed in order to estimate evaporative emissions from canister-equipped vehicles [9-12]. These models considered several factors such as vehicle design (tanks), ambient temperature, driving conditions, or gasoline volatility [13] but there is a lack of experimental confirmation of the relationship between canister performance, gasoline composition and the characteristics of the adsorbent, as indicated by Yamada [9]. Activated carbons (ACs) are the most widely used adsorbent due to the fact that both their porous and chemical nature can be easily tailored. Moreover, cheap ACs can be produced from raw materials such as agricultural residues [2, 5, 17, 18]. In comparison, zeolites are about ten times more expensive [19].

In this work, we prepared a series of ACs from olive stones. We developed the porous texture by chemical activation and modified the surface chemistry by means of a severe oxidation process. After that, a selective removal of oxygenated surface groups was performed in order to find out more about specific VOC-AC interactions, which may affect the adsorption and regeneration capacities. Ethanol and n-octane were selected as target VOCs because they are the main components of gasoline and have different chemical natures (ethanol is hydrophilic and n-octane is hydrophobic). Finally we correlated the evolution of porosity and chemical surface characteristics for these activated carbons with their ethanol and n-octane adsorption performance under static and dynamic conditions.

2. Materials and methods

2.1. Activated Carbon synthesis by KOH activation

Olive stones were milled and sieved to 1.0 – 2.0 mm, treated with sulfuric acid (1 N) in order to remove any remains of the pulp and then washed until all sulfates had been removed. A two-stage activation procedure was designed: initially, olive stones were carbonized at 400 ºC for two hours under a nitrogen flow (300 cm^3 min^{-1}) and then the char obtained was chemically activated using a mixture of char and KOH in a 1:7 mass ratio. This mixture was treated under nitrogen flow (300 cm^3 min^{-1}) for two hours at 350 ºC followed by three hours at 850 ºC (heating rate 10 ºC min^{-1}). The sample was kept under nitrogen atmosphere while it was cooled to room temperature. Finally, it was treated with HCl and HF, which also removed the excess base (KOH), washed with distilled water till all chlorides had been removed and dried in an oven at 110 ºC for 24 hours before storage. This sample was called CA.

2.2. Chemical surface modifications

Ammonium peroxydisulfate ($(NH_4)_2S_2O_8$) was chosen as the oxidizing agent [20]. CA was mixed with a saturated solution of this salt on H_2SO_4 1 M. After 24 hours under stirring at room temperature, oxidized carbon was filtered and washed with distilled water several times until all sulfates had been removed. This material was dried at 110 ºC and labeled as CAOX. Thermal treatments under nitrogen atmosphere (150 cm^3 min^{-1}) at 300 ºC, 500 ºC and 700 ºC (10 min, 20 ºC min^{-1}) were carried out on different portions of CAOX in order to selectively remove oxygenated surface groups (OSG). These samples were labeled as CAOX300, CAOX500 and CAOX700.

2.3. Textural Characterization.

The corresponding N_2 and CO_2 adsorption isotherms at -196 ºC and 0 ºC were obtained using an AUTOSORB 1 (QUANTACHROME Ins.) instrument. Parameters such as BET surface area, micropore volume (W_0) and micropore mean width (L_0) were calculated by applying BET, Dubinin-Radushkevich and Stoeckli equations to isotherms [21, 22]. Pore size distribution (PSD) curves were obtained by DFT or BJH derived methods [23, 24]. Mesopore volume (V_{meso}) was estimated considering the total pore volume as the volume of nitrogen adsorbed at a relative pressure $P/P_0 = 0.95$ ($V_{0.95}$). Therefore, V_{meso} was obtained from the difference between $V_{0.95}$ and W_0 (N_2). Mercury pycnometry was carried out in order to determine the apparent density of samples. In preparation for this procedure, samples were previously degasified at 110 ºC under dynamic vacuum (10^{-3} Torr).

2.4. Chemical Characterization

Thermal Programmed Desorption (TPD) curves of carbon monoxide and carbon dioxide were recorded. The analysis of TPD profiles enabled us to quantitatively determine the total oxygen content and the number of different oxygenated groups. The assignment of these groups was based on the bibliography [25-28]. Experiments were carried out by heating around 150 mg of sample at 50 K min^{-1} up to 1273 K using He as the carrier gas (60 cm^3 min^{-1}). The analysis of desorbed gases was performed with a Mass Spectrometer model Prisma (Pfeiffer).

X-ray photo emission spectra (XPS) were recorded using a Kratos Axis Ultra-DLD spectrometer. As a radiation source this instrument uses MgKα (hν = 1253.6 eV) and a hemispheric electron analyzer operating at 12 kV and 10 mA. Since we wanted to

quantify total oxygen content, we analyzed regions for C_{1s} and O_{1s}. The deconvolution of spectra and the assignment of bands were also performed according to the bibliography [28, 29].

Zero-point charge pH (pH_{ZPC}) of samples was determined with the method proposed by Leon et al. [30]. Approximately 250 mg of each sample were suspended on 4 mL of distilled water previously degasified. Suspensions were stirred and thermostated at 25 ºC measuring the pH periodically until readings were constant. The final pH obtained this way was considered as the pH_{ZPC} for each sample.

2.5. VOC adsorption

a) Static adsorption

Ethanol and n-octane static adsorption experiments were carried out by exposing 0.050 g of each sample, previously dried at 110 ºC, in a desiccator containing ethanol (absolute ethanol, Panreac) or n-octane (octane ≥99% GC, Sigma-Aldrich) at room temperature (≈ 25 ºC) (P_0 = 57 and 16 Torr respectively). In these experiments, samples were placed in a saturated atmosphere of the organic vapor until equilibrium was reached, and then the total adsorption capacity of the samples was determined [3, 4]. Samples were weighed daily till constant weight by using a Denver Instruments SI-234 balance with an accuracy of 0.1 mg. VOC desorption was studied by DSC and TG with a METTLER-TOLEDO TGA/DSC1, heating VOC-saturated samples under N_2 flow (60 cm^3 min^{-1}) to 500 and 950 ºC respectively (10 ºC min^{-1}). Desorbed amounts of VOC and desorption energies were determined and correlated with the textural and chemical characteristics of the samples.

b) Dynamic adsorption

Breakthrough curves were determined by using the instrumental set-up described in Figure 1. Breakthrough columns consist of a U-shaped reactor (0.4 cm inner diameter) containing 0.1 g of adsorbent fixed bed. ACs were pretreated at 200 ºC under He flow (60 cm^3 min^{-1}) for one hour, and then, breakthrough adsorption curves were obtained at controlled temperature by changing from a He flow to an air/VOC flow (60 cm^3 min^{-1}, 480 ppm n-octane or 560 ppm ethanol). VOC concentration was fitted by bubbling the air flow through liquid VOC at 0 ºC and diluting with pure air in the appropriate proportion. VOC concentration was determined by a Gas Chromatograph CP-3800 (VARIAN) equipped with a Carbowax-20M column and FID detection.

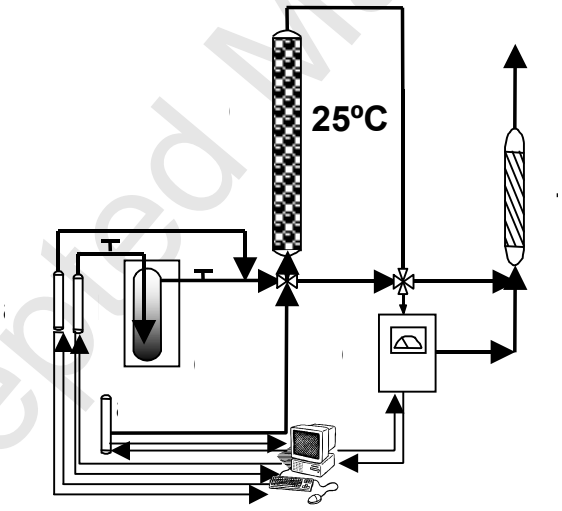

Figure 1. a) Mass flux controllers for He and air flows b) VOC reservoir c) Cryostat d) AC column e) Gas chromatograph f) Waste trap

The analysis of breakthrough curves was performed using the mass transfer zone (MTZ) concept [31, 32]. Different parameters may be determined from the analysis of breakthrough curves: breakthrough ($V_{0.02}$) and saturation ($V_{0.90}$) points that are defined as eluted volumes when the VOC concentration at the column exit reached values of 2

and 90% of the initial VOC concentration (expressed as time on stream or volume treated), the amount adsorbed at these points $X_{0.02}$ and $X_{0.90}$, the mass transfer zone height (H_{MTZ}) and the rate at which MTZ moved forward (R_{MTZ}).

The mass transfer zone (MTZ) and the mass transfer zone height (H_{MTZ}) are defined as the region of the bed within which the adsorption process is taking place. MTZ is therefore located between the saturated part of the bed and the clean part. This means that there is a VOC concentration gradient which moves with the MTZ along the adsorbent bed to the end column. Diffusion and adsorption are happening at the same time. Therefore, values of H_{MTZ} are smaller for rapid adsorption than for slow adsorption. The calculation of this parameter was carried out by applying the following equation described in the bibliography [33]:

$$H_{ZTM} = h\left(\frac{V_{0.90} - V_{0.02}}{V_{0.02} + \phi(V_{0.90} - V_{0.02})}\right) \qquad \phi = \frac{\int_{V_{0.02}}^{V_{0.90}} (C_0 - C)dV}{C_0(V_{0.90} - V_{0.02})}$$

Where $V_{0.02}$ and $V_{0.90}$ have been already defined, h is the height of the adsorption bed and ϕ is the fractional capacity which is related to the efficiency of the adsorption process within the MTZ and is calculated using the equation shown above on the right.

As adsorption occurs, part of the adsorbent is saturated and the MTZ moves forward, so enabling us to calculate the mass transfer zone displacement rate (R_{MTZ}). This is done by multiplying H_{MTZ} by the flow rate and then dividing by the difference between breakthrough and saturation volumes.

3. Results and discussion

3.1. Textural characterization

The textural characteristics of the samples were determined by analyzing N_2 and CO_2 adsorption isotherms. The results are summarized in Table 1 and the PSD obtained from N_2 adsorption isotherms (QSDFT analysis) is shown in Figure 2. The high KOH:carbon ratio led to a high activation degree (44 % wt.). The original CA therefore showed a high micro/mesopore volume and surface area values (Table 1). CA oxidation led to the destruction of about 50 % of porosity ($V_{0.95}$). This explains the big difference in apparent density between the two samples (CA, 0.20 g cm^{-3} and CAOX, 0.41 g cm^{-3}). After thermal treatments this parameter slowly decreased.

Textural transformations clearly took place above all within the mesopore range (Figure 2 and Table 1). The original PSD of the CA sample presents a maximum for mesopores with diameters between 2.8 - 3.0 nm and a maximum for micropores of around 0.8 nm in diameter, indicated in the latter case by the small peak of the PSD curve.

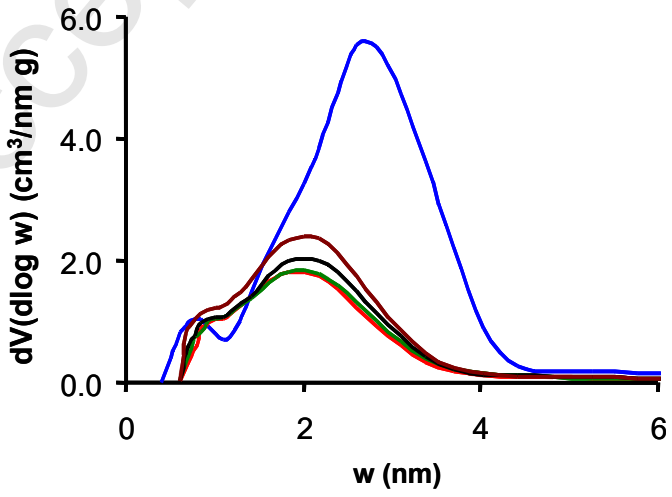

Figure 2. Pore size distributions obtained by applying the QSDFT method to the corresponding N_2 adsorption isotherm. CA (blue), CAOX (red), CAOX300 (green), CAOX500 (black), CAOX700 (brown).

Original mesopores were destroyed by the oxidation process and transformed into macropores (not detected by N_2 adsorption). The pore destruction becomes progressively smaller as pore size decreases: V_{meso} decreases by 52 % and, at the micropore range, W_0 (N_2) decreases by 32 % while the narrowest micropores, W_0 (CO_2), determined by CO_2 adsorption [34], increase by around 10 %. This pore volume reduction also leads to a drastic reduction of S_{BET} from 2387 to 1661 $m^2\ g^{-1}$.

Nevertheless, not only pore destruction occurred. Oxygen surface groups (OSG) were also partially blocking the porosity in the same range (large micropores and mesopores), thus after progressive thermal treatments at 300, 500, and 700 ºC, carried out to selectively remove these OSG, as will be described below, W_0 (N_2), W_0 (CO_2) and V_{meso} increased, leading also to a simultaneous increase in S_{BET}. Thus there is a pore widening associated with the release of the OSG favoring large micropores and mesopores, which again shifts the PSD to the mesopore range. However, mesoporosity in the original pore range was never recovered (Figure 2).

Table 1. Textural properties of samples obtained by gas (N_2 and CO_2) adsorption.

Sample	S_{BET} $m^2\ g^{-1}$	W_0 (N_2) $cm^3\ g^{-1}$	W_0 (CO_2) $cm^3\ g^{-1}$	$V_{0.95}$ $cm^3\ g^{-1}$	V_{meso} $cm^3\ g^{-1}$
CA	2387	0.92	0.39	2.23	1.31
CAOX	1661	0.63	0.43	1.07	0.44
CAOX300	1686	0.63	0.44	1.10	0.47
CAOX500	1696	0.68	0.48	1.18	0.50
CAOX700	1972	0.78	0.48	1.34	0.56

3.2. Chemical characterization

In addition to porous texture, surface chemistry will also determine the nature and extent of interactions with target VOCs. We therefore extensively analyzed the surface chemistry of ACs using XPS, TPD and pH_{ZPC} experiments. The results are summarized in Table 2. Particularly noteworthy is the sharp increase in CA oxygen content after oxidation to CAOX, which also produced a strong acidification of the carbon surface as denoted by the variation in pH_{ZPC} values. Oxygenated surface groups are located inside pores (mainly large micropores and small mesopores, as previously commented) and thus $\%O_{TPD} > \%O_{XPS}$. By weighing each sample before and after thermal treatments, we observed a significant total weight loss due to the release of gases, reaching as high as 40% at 700 ºC , responsible for the surface development and pore widening described above.

Table 2. Chemical characteristics of samples from TPD, XPS and pH_{ZPC} analyses.

Sample	WL	CO	CO_2	O_{TPD}	O_{XPS}	pH_{ZPC}
	%	μmol g^{-1}	μmol g^{-1}	%	%	
CA	-	1160	150	2.3	1.7	7.5
CAOX	-	3680	3010	15.5	9.3	2.4
CAOX300	20	5070	2110	14.9	7.0	2.9
CAOX500	24	6030	1370	14.0	5.6	3.0
CAOX700	40	680	110	1.4	1.4	7.8

Information about the chemical nature of the OSG present in each sample was obtained by analyzing TPD profiles (Figure 3). This is because OSG are evolved at different temperature ranges and can therefore be identified and quantified (Table 2). The highest peak in the CO_2 profile of sample CAOX is located at 278 ºC and is attributed to the release of carboxylic acid groups. The strong shoulder at 450 ºC and the long tail of the CO_2-profile indicate that other CO_2-evolving groups, such as anhydrides and lactones, are present. Anhydrides may be formed from the dehydration of two neighboring carboxylic groups. Maximum CO-desorption takes place at 555 ºC, but this peak is very wide and has a long tail. This means that different CO-evolving groups may also be present. According to previous studies, phenols [25-27] evolve between 600-700 ºC, ether groups at around 700 ºC, carbonyls between 800-900 ºC and more stable chromenes at around 1000 ºC. However, Marchon [35] tentatively assigned different peaks and the CO-profile shoulder to semiquinone functional groups on energetically different sites.

As published in a previous paper [27] oxygenated surface groups are selectively removed at different temperature ranges, and the oxygen content decreases linearly as the treatment temperature increases. Nevertheless, it is important to note the exceptional behavior of CAOX after treatments between 300-500 ºC. Thus, as can be seen in Table 2, $\%O_{XPS}$ progressively decreases in contrast to $\%O_{TPD}$, which remains practically unchanged at this temperature range. After treatments at 700 ºC, the oxygen content fell sharply and CAOX700 showed a similar surface chemistry to the original CA. Therefore, there is a dramatic reorganization of OSG inside the pores in the 300 – 500 ºC range. It is remarkable that even at the lower temperature (300 ºC), the treatment is strong enough to completely eliminate the carboxylic acid groups present in the CAOX sample (Figure 3). CO_2 evolved in this process from both CAOX300 and CAOX500 is mainly reincorporated forming CO-evolving groups (semiquinone) that are also progressively more stable, as indicated by the CO-peak shifting to higher temperatures.

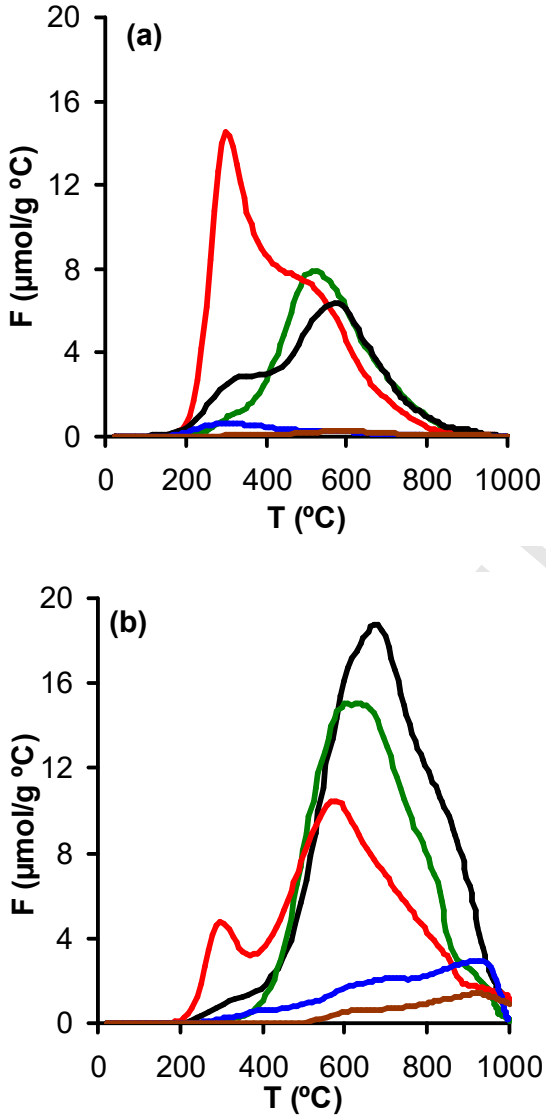

Figure 3. TPD curves for CO_2 (a) and CO (b). CA (blue), CAOX (red), CAOX300 (green), CAOX500 (black), CAOX700 (brown).

3.3. Adsorption of n-octane and ethanol

3.3.1 Static adsorption

The objective of this study was to develop specific traps for VOCs. Adsorption capacities determined under static conditions at 25 ºC are summarized in Table 3. Results are expressed as liquid volume, considering n-octane and ethanol density values as 0.703 and 0.791 g cm^{-3} respectively, to facilitate correlations with pore volumes. It is interesting to note that these adsorption values are a very good match for the total pore volume ($V_{0.95}$) of the samples. It is also noteworthy that the adsorption values for our samples are significantly higher than for other adsorbents [36], including activated carbons [37]. Thus, for example, BASF activated carbon with a micropore volume of 0.39 cm^3 g^{-1} and a macropore volume of 0.31 cm^3 g^{-1} has an ethanol adsorption capacity of 0.43 cm^3 g^{-1} at a relative pressure of 0.9 and 25 ºC [37]. In our case, the ethanol adsorption capacity of CA was enhanced by the presence of mesopores (instead of macroporosity on BASF carbon), in agreement with previously observed results [3] for toluene adsorption. The developed porosity of the CA sample favors both the higher adsorption capacities and the desorption energies (E_d), determined from DSC-experiments, of the samples series (Table 3). N-octane adsorption seems to be favored compared to ethanol adsorption by the mainly hydrophobic character of the carbon surface, which means that E_d is smaller.

The adsorption capacity decreases for both ethanol and octane after oxidation due to the huge porosity destruction mentioned earlier. The hydrophilic surface of CAOX now favors ethanol adsorption relative to n-octane, E_d takes the maximum value of the samples series for ethanol adsorption, and the minimum value for n-octane adsorption. Curiously, sample CAOX presents a higher adsorption capacity (for both ethanol and

octane) than CAOX300. Given that they have similar textural properties (Table 1), the decrease in adsorption capacity must therefore be associated with chemical transformations (i.e. the release of carboxylic acid groups). Simultaneously, there is a sharp fall in the ethanol desorption energy (E_d), while the contrary effect is observed for octane. Thus carboxylic acids clearly favor interactions with ethanol and make those with n-octane more difficult. The CAOX300 and CAOX500 samples showed quite similar adsorption/desorption characteristics based on a similar total oxygen content ($\%O_{TPD}$) and pH_{ZPC}. This means that despite the substantial reorganization of OSG that takes place in these samples (decomposition of labile CO_2- evolving groups and formation of more stable CO-evolving groups, Table 2), interactions between adsorbates and these new OSG are less specific than those previously commented for carboxylic acid groups. When the treatment temperature is increased to 700 ºC, the pore opening and the increase in surface area again enhance the adsorption capacity of the samples.

There is also a good match between the adsorbed and desorbed amounts. This shows that the thermal regeneration of samples is effective and consequently that they can be reused in subsequent adsorption-desorption cycles. VOC desorption was carried out by heating during TG-experiments, and as a result OSG were simultaneously evolved, which could influence these results. In order to avoid these interferences, we also analyzed fresh samples, and the VOCs desorbed in the temperature range in fresh samples were shown to be thermally stable in terms of weight loss. Figure 4 shows some of the TG profiles for VOC desorption including the corresponding fresh samples.

Table 3. Adsorbed amounts of ethanol and n-octane at saturation under static conditions and the amounts desorbed by thermal treatments.

Sample	ethanol			n-octane		
	Adsorbed (cm^3g^{-1})	Desorbed (cm^3g^{-1})	Ed (kJ mol^{-1})	Adsorbed (cm^3g^{-1})	Desorbed (cm^3g^{-1})	Ed (kJ mol^{-1})
CA	2.35	2.04	61.1	2.60	1.99	23.5
CAOX	1.61	1.37	62.3	1.22	1.18	7.5
CAOX300	1.07	1.05	48.2	0.86	0.85	18.8
CAOX500	1.11	1.18	49.2	0.85	0.81	19.9
CAOX700	1.28	1.31	38.1	1.12	1.11	12.5

As can be observed in Figure 4, the CA samples saturated with ethanol (Figure 4a) and with n-octane (Figure 4e) both suffer a severe weight loss (WL) at low temperature, followed by a large plateau. Fresh CA shows good thermal stability up to around 550 ºC. The amount of CO_2 released is low and the observed WL above this temperature is due mainly to the release of CO-evolving groups (Figure 3), with the two curves more or less parallel. VOC desorption is therefore associated exclusively with the first part of the TG profile, where the WL is not influenced by OSG release. Consequently, the saturated sample can be regenerated at low temperature. It should also be pointed out however that the CAOX sample has the weakest OSG and the strongest interactions with ethanol. This sample is only stable up to around 200 ºC, from which the WL observed for the fresh sample (Figure 4) is primarily due to the elimination of carboxylic groups (Figure 3). Nevertheless, ethanol desorption clearly finished before

the carboxylic groups were eliminated (Figure 4b), and the TG profile of the saturated sample shows a small plateau between 150 – 200 ºC. The amount of ethanol desorbed from the CAOX sample decreases compared to that from CA, as mentioned above. Nevertheless, desorption occurs within a large temperature range, as a consequence of interactions between EtOH-carboxylic acid groups. In this case, the sample regeneration should be carried out carefully at temperatures of less than 200 ºC in order to preserve carboxylic groups which, as previously described, enhance the EtOH adsorption capacity. The small plateau detected for saturated CAOX becomes progressively larger when the pretreatment temperature increases (Figures 4 c and d), and in all cases, the WL curves associated to the OSG run quite parallel to each other in fresh and saturated samples. DSC profiles for the ethanol desorption from certain selected samples are also included in Figure 4. The desorption process is obviously endothermic, the DSC-peak of CAOX saturated samples shows a long tail at higher temperatures, due to the interaction of ethanol with carboxylic groups, which falls significantly after the treatment at 300 ºC (CAOX300).

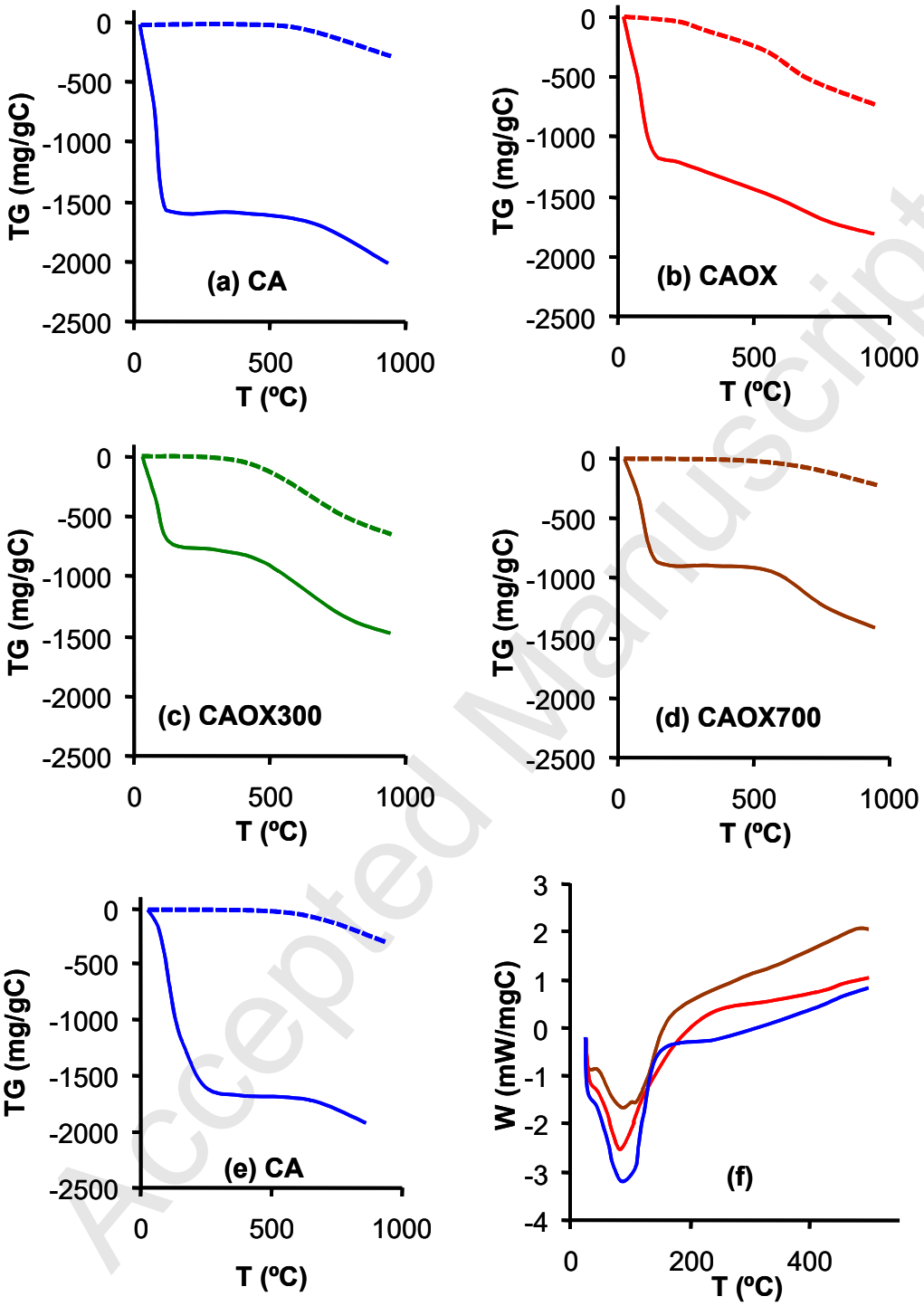

Figure 4. TG profiles of fresh (dash line) and VOC-saturated (a,b,c,d – ethanol, e - octane) samples (solid line). Figure 4 f. DSC curves for ethanol desorption.

3.3.2 Dynamic adsorption

In Figure 5, the behavior of samples as n-octane (Figure 5a) and ethanol (Figure 5b) adsorbents under dynamic experimental conditions is presented by the corresponding breakthrough curves. The parameters obtained from the analysis of these curves are summarized in Tables 4 and 5 for n-octane and ethanol respectively. The contrasting behavior of these samples when adsorbing the alkane or the alcohol is easy to observe. This behavior is related to the evolution of the textural and chemical properties discussed earlier and coincides with results obtained under static conditions. Previous studies of ACs and carbon fiber ethanol adsorption showed that the adsorption rate is determined by diffusion processes [38] and that the adsorption kinetics could be fitted to empirical correlations showing the influence of adsorption temperature and VOC concentration [39, 40]. In a previous article [3] we pointed out the strong influence of mesoporosity in carbon aerogels used as toluene adsorbents under static and dynamic conditions.

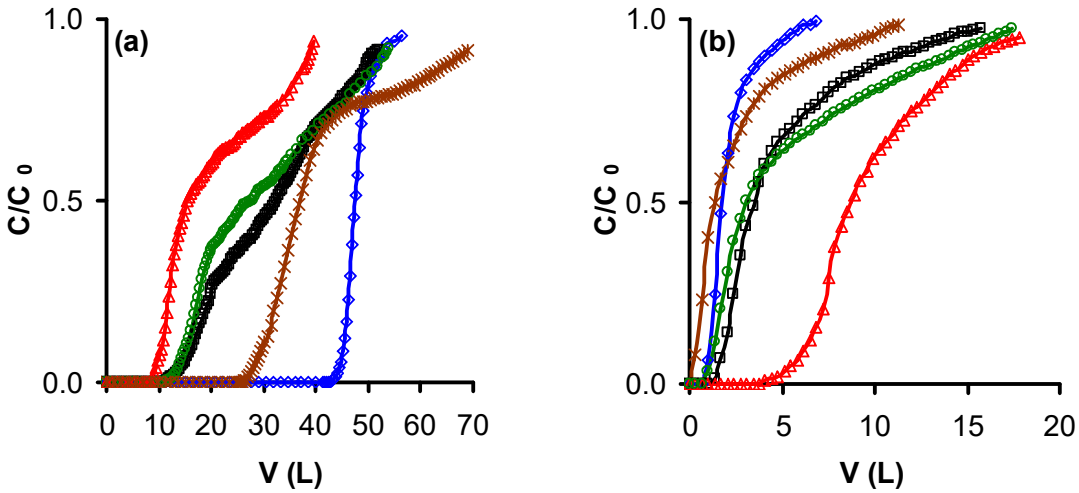

Figure 5. Breakthrough curves in dry air (a) n-octane (b) ethanol. CA (◆), CAOX (Δ), CAOX300 (○), CAOX500 (□), CAOX700 (×).

Clearly, within these experimental conditions the series of samples prepared is more specific for the adsorption of n-octane than of ethanol. Thus, in the worst case 43.7 mg g^{-1} of n-octane are adsorbed as compared to the 26.5 mg g^{-1} of ethanol adsorbed in the best case at the breakthrough point. Under these experimental conditions, the porosity involved in the adsorption processes is different than under static conditions, because of the smaller P/P_0, thus the volume of n-octane adsorbed approximately matches $W_0(CO_2)$ for CA and CAOX700 samples. These results agree with those observed by other authors [2]. The adsorption capacity strongly decreases for CAOX and gradually recovers after thermal treatments (Table 4). In the case of ethanol adsorption, the volume of ethanol adsorbed is significantly smaller than the micropore volume in all cases. The fact that more ethanol was adsorbed in the CAOX sample despite it having the smallest pore volume denotes that in this case adsorption is enhanced by chemical interactions.

After oxidation, the hydrophilic character of the CAOX surface increases [40], which favors ethanol adsorption but makes n-octane adsorption more difficult. Thus, the corresponding breakthrough curves appear before and after the original CA adsorption curve for n-octane and ethanol respectively. There is also an important change in terms of the curve shapes. For both pollutants the difference between breakthrough and saturation points increased compared to CA, and the curves showed important slope changes indicating changes in the accessibility of the pores and/or interactions with the

carbon surface. After removing the OSG, breakthrough curves tended to return to the shape and position of the original CA curves.

The BET surface area drops by 32 % from CA to CAOX, however, n-octane adsorption capacity decreases by about 78 % at the breakthrough point and 56% at the saturation point, which shows the influence of surface chemistry. The smaller n-octane - adsorbent interaction after oxidation is also indicated by an increase in the R_{MTZ}, which leads to an increase in the H_{MTZ} of 500 % with regard to the CA sample. Opposite effects are observed for ethanol adsorption: the increase of the adsorption capacity by a factor of four and the six-fold decrease of the R_{MTZ} are indicative of stronger ethanol - adsorbent interactions. These results are also in line with those previously obtained in static conditions and related with E_d variations (Table 3).

Table 4. Parameters obtained from the analysis of n-octane breakthrough curves.

Sample	Bed Height cm	$V_{0.02}$ L	$X_{0.02}$ mg g^{-1}	$V_{0.90}$ L	$X_{0.90}$ mg g^{-1}	H_{MTZ} cm	R_{MTZ} cm h^{-1}
CA	6.7	43.9	206.3	52.0	223.8	0.34	0.15
CAOX	4.2	9.0	43.7	38.8	99.0	1.73	0.21
CAOX300	4.2	13.1	62.5	53.2	146.6	1.57	0.14
CAOX500	4.1	13.9	66.9	51.9	158.5	1.37	0.13
CAOX700	4.1	27.1	130.0	67.6	198.7	1.17	0.10

After treatment at 300ºC, the release of carboxylic groups strongly decreases the adsorption of ethanol while enhancing that of n-octane. The specificity of these groups for ethanol adsorption is pointed out by the variation of the breakthrough point, $X_{0.02}$,

which decreases about fivefold (Table 5). It is also important to note that at this point ethanol adsorption is favored in the case of CAOX500 compared to CAOX300. This is probably due to the stronger regeneration capacity at this temperature of the carboxylic acid groups evolving at 280 ºC (Figure 3a). Smaller differences were observed at the saturation point, $X_{0.90}$ decreases by a half after treatment at 300 ºC, and only drops slightly after treatment at 500 ºC, in spite of the OSG reorganization mentioned earlier. This fact also highlights the unspecific character of CO-evolving groups, in contrast to that of carboxylic groups. For CAOX700 both $X_{0.02}$ and $X_{0.90}$ decrease in spite of the higher S_{BET}. The low affinity of the CAOX700 surface for ethanol is highlighted by the sharp increase in R_{MTZ}.

Table 5. Parameters obtained from the analysis of ethanol breakthrough curves.

Sample	$V_{0.02}$ L	$X_{0.02}$ mg g^{-1}	$V_{0.90}$ L	$X_{0.90}$ mg g^{-1}	H_{MTZ} cm	R_{MTZ} cm h^{-1}
CA	1.2	5.0	4.1	10.7	2.80	3.48
CAOX	4.6	26.5	15.6	53.4	1.72	0.56
CAOX300	0.9	5.2	14.0	28.4	3.02	0.83
CAOX500	1.5	8.0	11.1	25.5	2.53	0.95
CAOX700	0.2	1.2	7.0	12.0	3.80	3.80

N-octane adsorption is progressively enhanced with the elimination of oxygenated surface groups, although the n-octane adsorption capacity of CA is not recovered. The adsorption of n-octane is mainly determined by textural characteristics (Figure 6) while ethanol adsorption is more influenced by surface chemistry (Figure 7a), namely, by the

presence of carboxylic acid groups (Figure 7b). The stronger the interaction, the smaller the R_{MTZ} and H_{MTZ} in the corresponding fixed bed columns. Therefore, because the performance of the trap will depend on the nature and concentration of the VOCs and on the activated carbon porosity and surface chemistry, the preparation of traps for gasoline vapors based on mixtures of adsorbents could be an appropriate approach. We are currently studying this question in our laboratory, along with those of competitive adsorption and the influence of humidity in the stream.

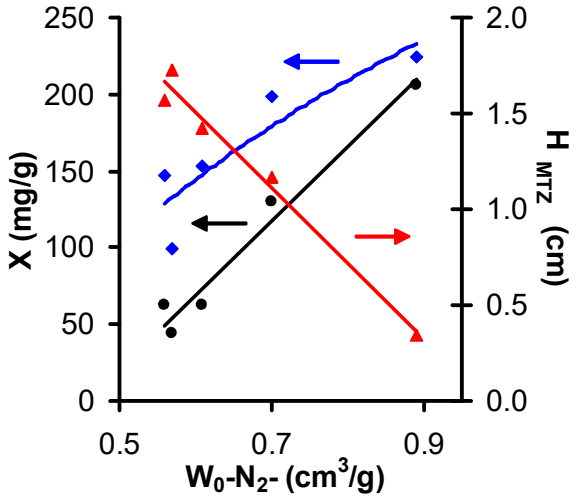

Figure 6. Variation of n-octane adsorption capacity, $X_{0.02}$(•), $X_{0.90}$(♦) and H_{MTZ} (▲) with the micropore volume of samples $W_0(N_2)$.

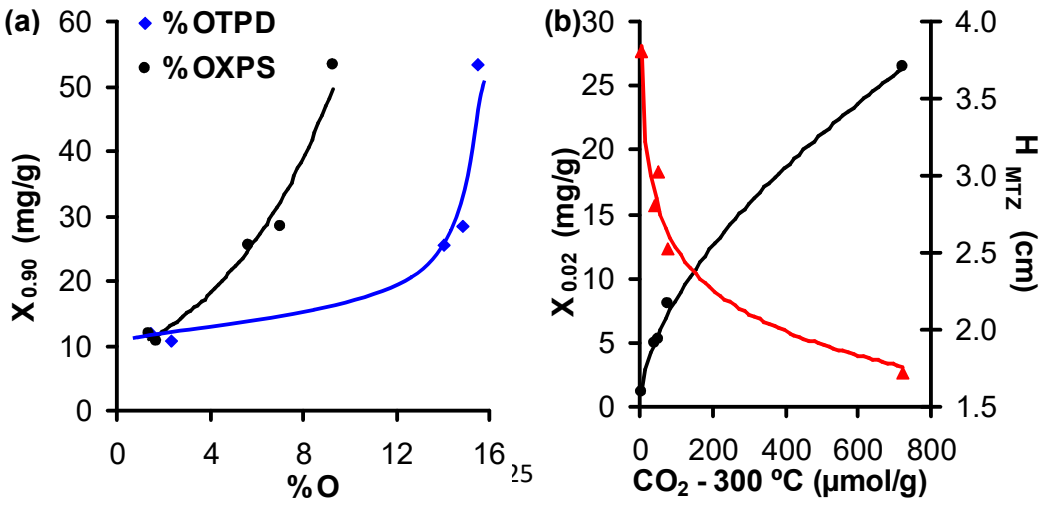

Figure 7. Variation of ethanol adsorption capacity. (a) Saturation point with oxygen content and (b) Breakthrough point $X_{0,02}$(•) and H_{MTZ} (▲) with CO_2 desorbed by samples up to 300ºC.

4. Conclusions

A highly porous activated carbon (CA) was obtained by means of chemical activation of carbonized olive stones. The surface chemistry was modified with an oxidation treatment (CAOX) reaching an oxygen content of 16% wt. Different types of oxygenated surface groups were identified by TPD and selectively removed by heating CAOX sample proportions at different temperatures. Treatments up to 500 ºC did not produce any significant changes in the oxygen content (determined by TPD) but OSG varied from CO_2 to CO-evolving groups. Treatment at 700 ºC prevented this OSG reorganization, since these groups are no longer stable at this temperature, and as a result the oxygen content fell sharply and pH_{ZPC} returned to basic values for CAOX700.

All samples performed well as ethanol and n-octane adsorbents, under both static and dynamic conditions. Nevertheless, the two compounds have different requirements. ACs working at a high relative pressure of VOCs under static conditions (such as in a canister connected to the car tank) can be saturated at room temperature using the complete porosity. Under these conditions, in spite of the fact that surface chemistry (carboxylic groups) enhances the interactions with ethanol, the main factor is clearly its highly developed meso-microporosity. TG experiments showed that spent adsorbents can be regenerated with oxygenated or aliphatic VOCs for these kind of samples below 200 ºC.

The development of traps working in a stream of polluted VOCs at low concentration (ppm) requires only highly microporous samples. The surface functionalization favors ethanol adsorption, but makes octane adsorption more difficult. Of the different OSG analyzed by TPD, carboxylic acid groups were shown to produce a specific effect on ethanol adsorption, although adsorption capacity depends on the total oxygen content (hydrophobicity) of the carbon surface. The stronger the interaction, the smaller the R_{MTZ} and H_{MTZ} in the corresponding fixed bed columns.

Acknowledgments

This work is supported by the MICINN-FEDER, project CTM2010-18889.

References

[1] F.I. Khan, A. Ghoshal, Removal of Volatile Organic Compounds from polluted air, Journal of Loss Prevention in the Process Industries 13 (2000) 527-545.

[2] J. Carratalá-Abril, M.A. Lillo-Ródenas, A. Linares-Solano, D. Cazorla-Amorós, Activated Carbons for the Removal of Low-Concentration Gaseous Toluene at the Semipilot Scale, Ind. Eng. Chem. Res. 48 (2009) 2066-2075.

[3] F.J. Maldonado-Hódar, C. Moreno-Castilla, F. Carrasco-Marín, A.F. Pérez-Cadenas, Reversible toluene adsorption on monolithic carbon aerogels, Journal of Hazardous Materials 148 (2007) 548-552.

[4] F.J. Maldonado-Hódar, Removing aromatic and oxygenated VOCs from polluted air stream using Pt–carbon aerogels: Assessment of their performance as adsorbents and combustion catalysts, Journal of Hazardous Materials 194 (2011) 216-222.

[5] A. Martínez de Yuso, M.T. Izquierdo, R. Valenciano, B. Rubio, Toluene and n-hexane adsorption and recovery behavior on activated carbons derived from almond shell wastes, Fuel Processing Technology 110 (2013) 1-7.

[6] S. Morales-Torres, A.F. Pérez-Cadenas, F. Kapteijn, F. Carrasco-Marín, F.J. Maldonado-Hódar, J.A. Moulijn, Palladium and platinum catalysts supported on carbon nanofiber coated monoliths for low-temperature combustion of BTX, Applied Catalysis B: Environmental 89 (2009) 411-419.

[7] R.A. Catalao, F.J. Maldonado-Hódar, A. Fernandes, C. Henriques, M.F. Ribeiro, Reduction of NO with metal-doped carbon aerogels, Applied Catalysis B: Environmental 88 (2009) 135-141.

[8] J. Wang, L. Jin, J. Gao, J. Shi, Y. Zhao, S. Liu, T. Jin, Z. Bai, C.Y. Wu, Investigation of speciated VOC in gasoline vehicular exhaust under ECE and EUDC test cycles, Science of The Total Environment 445–446 (2013) 110-116.

[9] H. Yamada, Contribution of evaporative emissions from gasoline vehicles toward total VOC emissions in Japan, Science of The Total Environment 449 (2013) 143-149.

[10] W.Q. Huang, J. Bai, S.H. Zhao , A.H. Lv, Investigation of oil vapor emission and its evaluation methods, Journal of Loss Prevention in the Process Industries 24 (2011) 178-186.

[11] G. Mellios, Z. Samaras, An empirical model for estimating evaporative hydrocarbon emissions from canister-equipped vehicles, Fuel 86 (2007) 2254-2261.

[12] K. Sato, N. Kobayashi, Adsorption and Desorption Simulation of Carbon Canister Using n-Butane as Model Compound of Gasoline, Journal of the Japan Petroleum Institute 54 (2011) 136-145.

[13] J.Y. Chin, S.A. Batterman, VOC composition of current motor vehicle fuels and vapors, and collinearity analyses for receptor modeling, Chemosphere 86 (2012) 951-958.

[14] http://www.api.org/environment-health-and-safety/environmental-performance/innovation/recovered-gas-vapors-add-value-cut-emissions.

http://www.api.org/environment-health-and-safety/health-safety/product-safety-home/safe-storage-and-disposal-of-gasoline

[15] R.K. Niven, Ethanol in gasoline: environmental impacts and sustainability review article, Renewable and Sustainable Energy Reviews 9 (2005) 535-555.

[16] M. Winther, F. Müller, T.C. Jensen, Emission consequences of introducing bio ethanol as a fuel for gasoline cars, Atmospheric Environment 55 (2012) 144-153.

[17] A. Baçaoui, A. Dahbi, A. Yaacoubi, C. Bennouna, F.J. Maldonado-Hódar, J. Rivera-Utrilla, F. Carrasco-Marín, C. Moreno-Castilla, Experimental Design To Optimize Preparation of Activated Carbons for Use in Water Treatment, Environmental Science & Technology 36 (2002) 3844-3849.

[18] A.S. Mestre, A.S. Bexiga, M. Proença, M. Andrade, M.L. Pinto, I. Matos, I.M. Fonseca, A.P. Carvalho, Activated carbons from sisal waste by chemical activation with K2CO3: Kinetics of paracetamol and ibuprofen removal from aqueous solution, Bioresource Technology 102 (2011) 8253-8260.

[19] H. Zaitan, D. Bianchi, O. Achak, T. Chafik, A comparative study of the adsorption and desorption of o-xylene onto bentonite clay and alumina, Journal of Hazardous Materials 153 (2008) 852-859.

[20] C. Moreno-Castilla, M.A. Ferro-Garcia, J.P. Joly, I. Bautista-Toledo, F. Carrasco-Marin, J. Rivera-Utrilla, Activated Carbon Surface Modifications by Nitric Acid, Hydrogen Peroxide, and Ammonium Peroxydisulfate Treatments, Langmuir 11 (1995) 4386-4392.

[21] R.G. Bansal, J.B. Donnet, F. Stoeckli, Activated Carbon, Marcel Dekker inc ed., New York and Basel, 1988.

[22] F. Stoeckli., Porosity in Carbon - Characterization and Applications, Eds. Patrick, J. ed. Arnold, London, 1995.

[23] E.P. Barrett, L.G. Joyner, P.P. Halenda, The Determination of Pore Volume and Area Distributions in Porous Substances. I. Computations from Nitrogen Isotherms, Journal of the American Chemical Society 73 (1951) 373-380.

[24] C. Lastoskie, K.E. Gubbins, N. Quirke, Pore size distribution analysis of microporous carbons: a density functional theory approach, The Journal of Physical Chemistry 97 (1993) 4786-4796.

[25] Y. Matsumura, Production of acidified active carbon by wet oxidation and its carbon structure, Journal of Applied Chemistry and Biotechnology 25 (1975) 39-56.

[26] J.L. Figueiredo, M.F.R. Pereira, M.M.A. Freitas, J.J.M. Órfão, Modification of the surface chemistry of activated carbons, Carbon 37 (1999) 1379-1389.

[27] C. Moreno-Castilla, F. Carrasco-Marín, F.J. Maldonado-Hódar, J. Rivera-Utrilla, Effects of non-oxidant and oxidant acid treatments on the surface properties of an activated carbon with very low ash content, Carbon 36 (1998) 145-151.

[28] J.H. Zhou, Z.J. Sui, J. Zhu, P. Li, D. Chen, Y.C. Dai, W.K. Yuan, Characterization of surface oxygen complexes on carbon nanofibers by TPD, XPS and FT-IR, Carbon 45 (2007) 785-796.

[29] C. Moreno-Castilla, A.F. Pérez-Cadenas, F.J. Maldonado-Hódar, F. Carrasco-Marín, J.L. Fierro, Influence of carbon–oxygen surface complexes on the surface acidity of tungsten oxide catalysts supported on activated carbons, Carbon 41 (2003) 1157-1167.

[30] C.A. Leon, J.M. Solar, V. Calemma, L.R. Radovic, Evidence for the protonation of basal plane sites on carbon, Carbon 30 (1992) 797-811.

[31] G.M. Luckchis, Adsorption systems 1. Design by mass-transfer-zone concept, Chemical Engineering 80 (1973) 111.

[32] W.J.J. Webber, *Physiochemical Processes for Water Quality Control*, Wiley-Interscience ed., New Cork, 1972.

[33] P.N. Cheremisinoff, F. Ellerbusch, Carbon Adsorption Handbook, Ann Arbor Science Pub. ed., Michigan, 1978.

[34] D. Cazorla-Amorós, J. Alcañiz-Monge, M.A. Casa-Lillo, A. Linares-Solano, CO2 As an Adsorptive To Characterize Carbon Molecular Sieves and Activated Carbons, Langmuir 14 (1998) 4589-4596.

[35] B. Marchon, J. Carrazza, H. Heinemann, G.A. Somorjai, TPD and XPS studies of O2, CO2, and H2O adsorption on clean polycrystalline graphite, Carbon 26 (1988) 507-514.

[36] A. Cartón, G.G. Benito, J.A. Rey, M. de la Fuente, Selection of adsorbents to be used in an ethanol fermentation process. Adsorption isotherms and kinetics, Bioresource Technology 66 (1998) 75-78.

[37] L. Gales, A. Mendes, C. Costa, Hysteresis in the cyclic adsorption of acetone, ethanol and ethyl acetate on activated carbon, Carbon 38 (2000) 1083-1088.

[38] B.B. Saha, I.I. El-Sharkawy, A. Chakraborty, S. Koyama, S.H. Yoon, K. Choon Ng, Adsorption Rate of Ethanol on Activated Carbon Fiber, J. Chem. Eng. Data 51 (2006), 1587-1592

[39] I.I. El-Sharkawy, B.B. Saha ,S. Koyama, K. Srinivasan, Isosteric heats of adsorption extracted from experiments of ethanol and HFC 134a on carbon based adsorbent Int. J. Heat and Mass Transfer 50 (2007) 902–907

[40] I.I. El-Sharkawy, B.B. Saha, S. Koyama, K. Choon Ng, A study on the kinetics of ethanol-activated carbon fiber: Theory and experiments, Int. J. Heat and Mass Transfer 49 (2006) 3104–3110

[41] F. Carrasco-Marín, A. Mueden, A. Centeno, F. Stoeckli, C. Moreno-Castilla, Water adsorption on activated carbons with different degrees of oxidation, Journal of the Chemical Society, Faraday Transactions 93 (1997) 2211-2215.

Highlights

1. High performance adsorbents of gasoline vapors as have been developed
2. The influence of their surface chemistry and porosity was determined
3. Ethanol adsorption is favored by specific interactions with carboxylic groups
4. VOC´s diffusion is favored by mesopores and the adsorption capacity by micropores
5. The VOC´s adsorbed is totally recovered by thermal regeneration

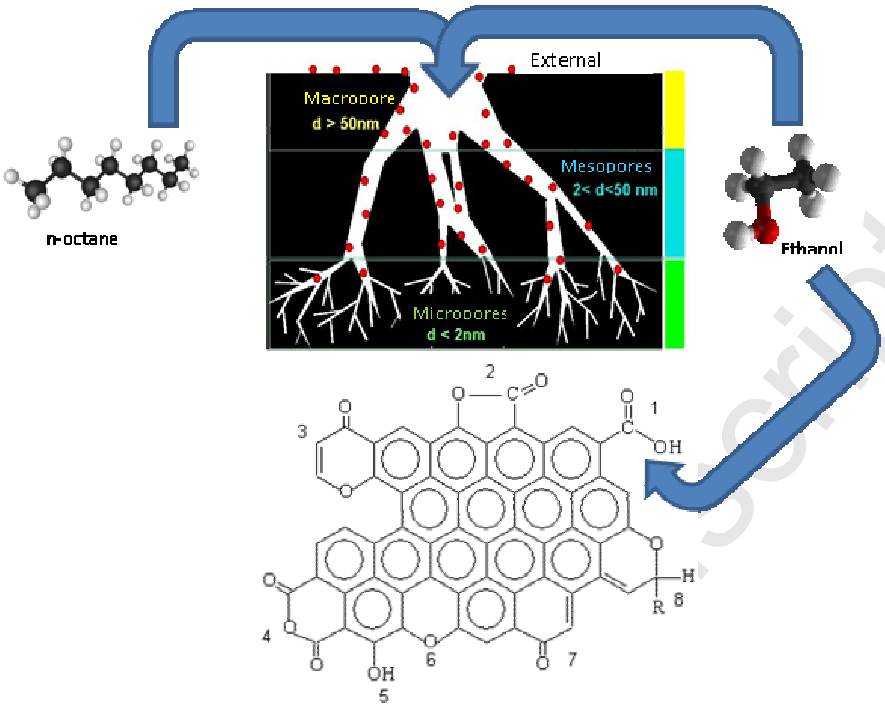

251658240